

Application of high-spatial-resolution secondary ion mass spectrometry for nanoscale chemical mapping of lithium in an Al-Li alloy

Xu Xu ^a, Chengge Jiao ^b, Kexue Li ^{a, c}, Min Hao ^d, Katie. L. Moore ^{a, c}, Timothy. L. Burnett ^{a, c, *}, Xiaorong Zhou ^a

^a School of Materials, University of Manchester, Manchester, M13 9PL, UK

^b Thermo Fisher Scientific, Achtseweg Noord 5, 5651 GG, Eindhoven, the Netherlands.

^c Photon Science Institute, University of Manchester, Manchester, M13 9PL, UK

^d Aluminium Alloys and Magnesium Alloys Research Institute, Beijing Institute of Aeronautical Materials, Beijing, 100095, China

*Corresponding author.

Email: timothy.burnett@manchester.ac.uk

Abstract

High-spatial-resolution secondary ion mass spectrometry offers a method for mapping lithium at nanoscale lateral resolution. Practical implementation of this technique offers significant potential for revealing the distribution of Li in many materials with exceptional lateral resolution and elemental sensitivity. Here, two state-of-the-art methods are demonstrated on an aluminium-lithium alloy to visualise nanoscale Li-rich phases by mapping the ${}^7\text{Li}^+$ secondary ion. NanoSIMS 50L analysis with a radio frequency O^- plasma ion source enabled visualisation of needle-shaped T_1 (Al_2CuLi) phases as small as 75 nm in width. A compact time-of-flight secondary ion mass spectrometry detector added to a focused ion beam scanning electron microscope facilitated mapping of the T_1 phases down to 45 nm in width using a Ga^+ ion beam. Correlation with high resolution electron microscopy confirms the identification of T_1 precipitates, their sizes and distribution observed during SIMS mapping.

Key words

Nanoscale mapping of lithium, high-spatial-resolution secondary ion mass spectrometry, NanoSIMS, FIB ToF-SIMS, aluminium-lithium alloy

Main text

The characterisation of lithium (Li) has received considerable attention from multiple disciplines in materials science in particular researchers working on the development of Li-ion battery materials and high-strength, low-density Al-Li alloys¹⁻⁹. High-spatial-resolution chemical mapping of Li is of particular interest in the case of Li-ion battery materials for investigating Li ion transport on the electrodes with nanoscale structures^{1,8,9}. It also offers excellent potential for revealing the distribution of nanoscale Li-rich precipitates in Al-Li alloys to understand their influence on mechanical and corrosion performance⁴⁻⁷. However, the analysis of Li is challenging as many techniques, such as energy dispersive X-ray spectroscopy (EDX or EDS) and X-ray photoelectron spectroscopy (XPS), have low elemental sensitivity for Li and/or insufficient spatial resolution^{3,10}. While the use of electron energy loss spectroscopy (EELS) and atom probe tomography (APT) enables the characterisation of Li with high spatial resolution if carried out with great care, these techniques are only able to cover extremely small areas due to the complexity of sample preparation and small sampling volume (e.g. $\sim 1 \times 10^{-2} \mu\text{m}^2$ and $\sim 5 \times 10^{-3} \mu\text{m}^3$ for EELS mapping and APT, respectively)^{11,12}.

Secondary ion mass spectrometry (SIMS) is a surface analysis technique that provides detailed chemical analysis and has been used widely on solid materials¹³. Elemental, isotopic and molecular information can be obtained from the top surface of a solid sample after bombardment by incident primary ions. The sputtered secondary ions are then extracted, transported and separated by a mass spectrometer according to their mass-to-charge ratio. SIMS offers excellent elemental sensitivity, in the parts per million to parts per billion range, in combination with the ability to detect light elements, including hydrogen, as well as isotopes from areas measuring 10's -100's μm ^{14,15}. This technique offers excellent potential for obtaining statistically meaningful information with a very high elemental sensitivity of Li, as it is an electropositive element with a high ionisation probability. However, the application of SIMS instruments is typically limited to a lateral resolution of $\sim 1 \mu\text{m}$ ¹⁻⁷, which is insufficient for revealing the details of Li distribution at the nanoscale.

The development of high-spatial-resolution SIMS instruments in recent years has facilitated imaging of Li distribution with a lateral resolution in the sub-micron range.

For instance, researchers using the NanoSIMS 50L (Cameca, France), using a Cs^+ primary ion beam with an impact energy of 16 keV and a lateral resolution of ~ 100 nm, were able to perform nanoscale analysis of Li in LiCoO_2 -based battery cathode materials by mapping $^7\text{Li}^{16}\text{O}^-$ to investigate the elemental distribution and the change of surface chemistry during electrochemical cycling⁸. A recently-developed compact design of time-of-flight (ToF) SIMS analyser (TOFWERK, Switzerland) added to a focused ion beam-scanning electron microscope (FIB-SEM) was also used to resolve the segregation of Li on grain boundaries and interfaces of particles in the $\text{LiNi}_x\text{Mn}_y\text{CO}_{1-x-y}\text{O}_2$ cathodes with a lateral resolution of ~ 50 nm^{9,16}. The use of a Zeiss ORION NanoFab Helium/Neon ion microscope equipped with a 25 keV He^+ primary ion source and a magnetic mass spectrometer has achieved a lateral resolution of 10 nm by mapping $^7\text{Li}^+$ in a lithium titanate and magnesium oxide nanoparticle mixture^{17,18}.

In addition, SIMS has been demonstrated as a potential method for characterising the distribution of nanoscale Li-rich precipitates in Al-Li alloys. However, most of the existing analyses are limited to a lateral resolution of $1 \text{ c } 10 \mu\text{m}$ ⁴⁻⁷ and were not able to spatially resolve the nanoscale phases. An early attempt was made utilising a laboratory-based SIMS instrument developed at the University of Chicago in collaboration with Hughes Research Laboratories (UC-HRL SIM, USA) to spatially resolve the nanoscale δ precipitates that are ~ 100 nm in diameter in an Al-10.7 at. % Li alloy^{19,20}. However, the practical implementation of modern commercialised high-spatial-resolution SIMS instruments for nanoscale chemical mapping of Li is rarely reported for Al-Li alloys.

The main aim of the present study is to investigate the capability of two of the high-spatial-resolution SIMS instruments for performing nanoscale chemical mapping in an Al-Li alloy with a particular focus on Li. The SIMS instruments employed are a NanoSIMS 50L (Cameca, France) system and a Ga^+ FIB time-of-flight secondary ion mass spectrometry (ToF-SIMS) instrument that comprises a Thermo Scientific Helios Tomahawk ion column FIB-SEM with a compact ToF-SIMS (TOFWERK, Switzerland) analyser. The results of SIMS analysis are further validated by correlative electron microscopy.

The material investigated in this study was an Al-Li-Cu-Mg alloy. The as-cast material

was hot-rolled to a thickness of 50 mm and then solution treated, followed by water quenching to room temperature. The material was then pre-stretched at room temperature, followed by a peak ageing treatment (T8) to facilitate the formation of nanoscale strengthening precipitates including δ' (Al_3Li) and T_1 (Al_2CuLi) phases. Samples for SIMS analysis were extracted from the rolling plane at the mid-thickness (T/2) position. The samples were prepared by grinding with SiC and water, sequential polishing with 3 μm and 1 μm diamond suspensions and a final chemo-mechanical polishing in a diluted solution of 1:1.5 oxide polishing suspension (OPS) to deionised water to give a surface finish without topographical artefacts.

Nanoscale chemical mapping was performed using NanoSIMS 50L and FIB ToF-SIMS in separate regions. The observations obtained from the SIMS analyses were further validated using correlative electron microscopy. This involved backscattered electron (BSE) imaging of secondary phase particles, grain orientation mapping by electron backscatter diffraction (EBSD) and high-resolution analysis using transmission electron microscopy (TEM) on a plan-view thin-foil specimen prepared using a Thermo Scientific Helios Xe^+ plasma FIB-SEM. Details of the procedure used for SIMS analysis and correlative electron microscopy are provided in supporting information.

Figure 1 shows the SIMS chemical maps obtained using NanoSIMS and FIB ToF-SIMS over an area of $35 \times 30 \mu\text{m}$ at a pixel size of 68.4 nm. The correlative BSE micrographs collected from the same regions with a pixel size of 34.2 nm are shown in Figures 1b and 1d.

The SIMS maps collected using NanoSIMS and FIB ToF-SIMS (Figures 1a and 1c) both reveal a clear $^7\text{Li}^+$ signal from the needle-shaped T_1 phases. Whilst as expected the majority of the constituent intermetallic phases show a lower level of $^7\text{Li}^+$ signal than the surrounding matrix. The observation of T_1 and constituent intermetallic phases is validated by BSE imaging in the same regions, Figures 1b and 1d. This is also consistent with our prior knowledge of the expected phases based on alloy composition and thermomechanical processing. These phases are clearly visualised with distinctive contrast differential to the surrounding matrix due to the abundance of heavier elements such as Cu²¹.

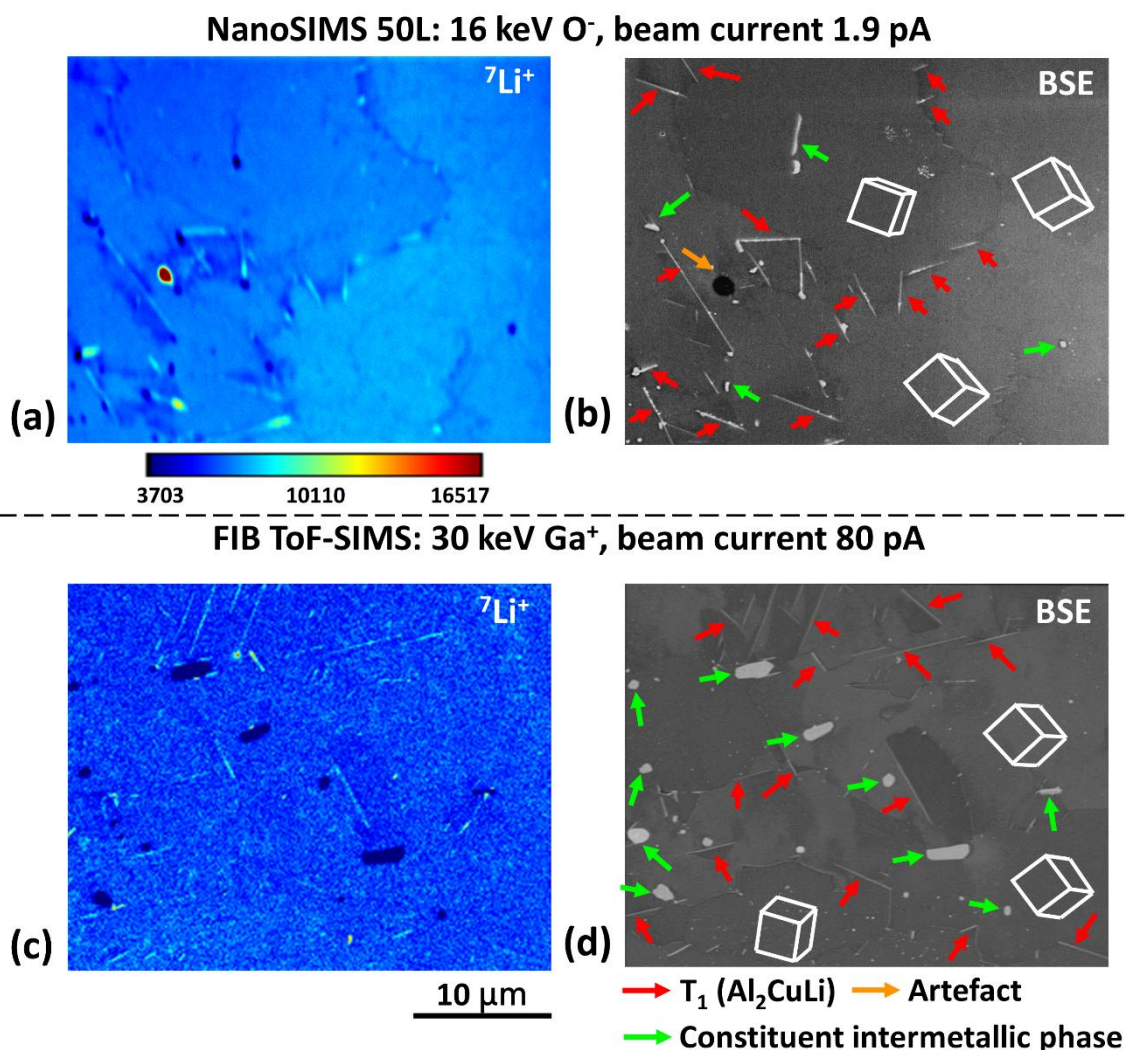


Figure 1. (a) NanoSIMS and (c) FIB ToF-SIMS chemical maps showing the distribution of ⁷Li⁺ and (b, d) the correlative BSE micrographs obtained after SIMS analysis. The arrows and insets in (b, d) indicate the secondary phase particles present in the area of interest and the crystal orientation measured by EBSD. The colour scale in (a) is presented based on counts per pixel. The count rates of secondary ion signal for both datasets from NanoSIMS and FIB ToF-SIMS are summarised in Table S1.

Figure 2 shows the results of higher resolution SIMS analysis conducted using the FIB ToF-SIMS instrument with a beam current of 24 pA and a pixel size of 29.3 nm. The correlative BSE micrographs collected from the same region with a pixel size of 14.6 nm are shown in Figures 2e and 2f.

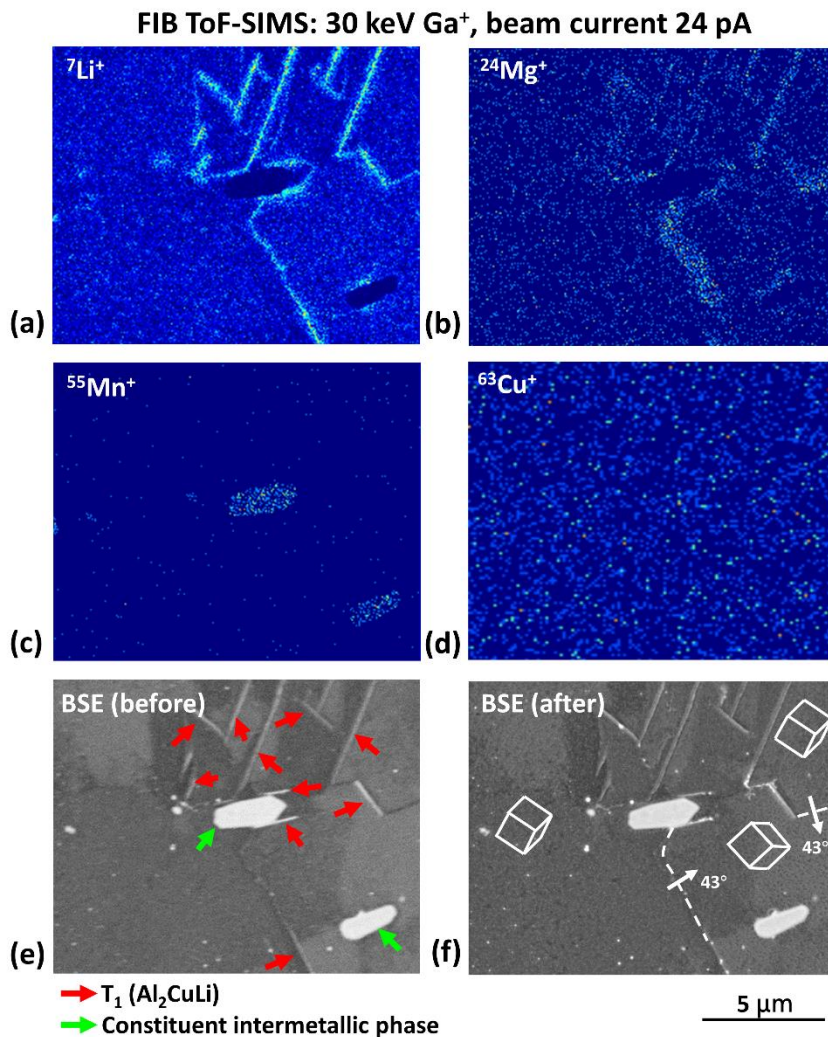


Figure 2. (a-d) The FIB ToF-SIMS chemical maps showing the distribution of ⁷Li⁺, ²⁴Mg⁺, ⁵⁵Mn⁺ and ⁶³Cu⁺ and (e, f) the correlative BSE micrographs obtained prior to and after SIMS analysis. The arrows in (e) indicate the secondary phase particles present in the areas of interest. The overlays and arrows in (f) indicate the crystal orientation and misorientation of grain boundaries measured by EBSD, respectively.

The observations of constituent intermetallic phases and the large T₁ phases are consistent with the result of FIB ToF-SIMS analysis conducted using a beam current of 80 pA (Figure 1c). In addition, the higher lateral resolution FIB ToF-SIMS chemical maps, Figures 2a and 2b, reveal segregation of Li and Mg on high angle grain boundaries (indicated in Figure 2f by the dashed lines) measuring ~ 90 nm in width. Constituent intermetallic phases exhibit a higher ⁵⁵Mn⁺ signal than the surrounding matrix, Figure 2c.

Figure 3 shows the ⁷Li⁺ SIMS chemical maps and BSE micrographs from magnified

regions and the line profiles showing the $^7\text{Li}^+$ signal variation across T_1 phase particles.

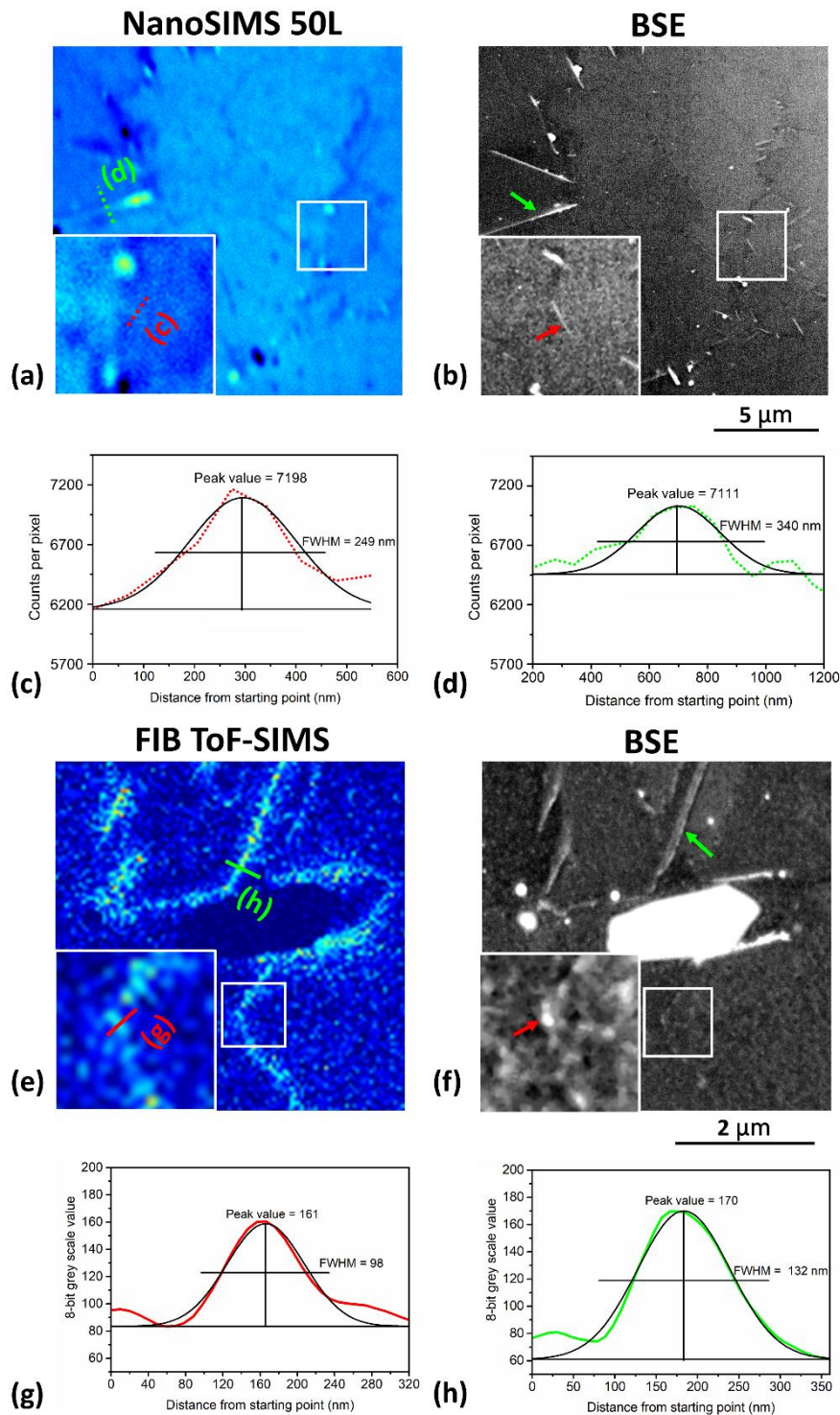


Figure 3. (a, e) $^7\text{Li}^+$ SIMS chemical maps detailing the distribution of Li within the regions analysed using the NanoSIMS and FIB ToF-SIMS instruments and (b, f) the post SIMS-analysis BSE micrographs from the same regions. The lines in (a, e) indicate the locations where intensity profiles were extracted. The arrows in (b, f) indicate the T_1 phase particles examined in detail. The insets

show the T_1 phase particles in magnified views. (c, d, g, h) Graphs showing the intensity profiles across the particles of interest. The black lines show the curves of Gaussian fit as applied using the Origin software for the measurement of full width half maximum (FWHM).

Intensity profiles with a line thickness of 1 pixel were extracted from the $^7\text{Li}^+$ chemical maps across the lines shown in Figures 3a and 3e, with the line profiles shown in Figures 3c, 3d, 3g and 3h. The profiles indicate that the widths of the particles measured by NanoSIMS are 249 nm (red) and 340 nm (green) using the full width half maximum (FWHM) method. The lateral resolution of NanoSIMS was further estimated to be 142 nm based on the 16 – 84% criterion (see Figure S1). In the FIB ToF-SIMS image, the particles measure 98 nm (red) and 132 nm (green) using the FWHM method. The lateral resolution of FIB ToF-SIMS was estimated to be 64 nm for the same beam current of 24 pA based on the measurement of lateral resolution from BAM 200L standard (see Figure S2). The T_1 phase particles analysed using line profiles were further correlated with the high resolution BSE micrographs from the same regions, Figures 3b and 3f. In Figure 3b the particles indicated by the red and green arrows were clearly visualised and measured ~ 75 nm and ~ 130 nm (FWHM) in width, respectively. In Figure 3f the particles indicated by the red and green arrows measured ~ 45 nm and ~ 120 nm (FWHM) in width, respectively.

The results of FIB ToF-SIMS analysis demonstrating the segregation of Li and Mg have been validated by S/TEM observations of the T_1 precipitates at the grain boundary. As demonstrated in Figure S4, the intragranular T_1 precipitates that are < 50 nm in length and 1 – 2 nm in width are too small to detect using either SIMS instrument. However, the grain boundary T_1 precipitates are formed as clusters that are continuously distributed on the grain boundary, Figure S4a. The clusters measure ~ 90 nm in width, which is consistent with the measured values of widths for the segregated regions showing a strong intensity of $^7\text{Li}^+$ signal as shown in Figure 2a. In addition, the T_1 phase particles measure 200 – 300 nm in length, which is similar to the lengths of Li-rich particles in the FIB ToF-SIMS $^7\text{Li}^+$ map as shown in Figure 3e. This confirms that the segregation of Li as observed using FIB ToF-SIMS corresponds to the clusters of Li-rich T_1 precipitates on the grain boundary.

In summary, the potential of advanced high-spatial-resolution SIMS instruments to

achieve chemical mapping with nanoscale lateral resolution has been shown by mapping ${}^7\text{Li}^+$ in Al-Li alloys. Li is challenging to detect with many characterisation techniques, but the results presented here show that it is possible to not only map Li but localise it with very high lateral resolution. NanoSIMS analysis was able to resolve features as small as 75 nm in size, whilst FIB ToF-SIMS could visualise the Li in T_1 phases as small as 45 nm in size, although neither technique could detect the intragranular precipitates that are smaller in size. The implementation of high-lateral-resolution SIMS instruments for characterising the distribution of Li in modern Al-Li alloys is of significant importance for understanding the influence of microstructure on mechanical and corrosion behaviour. It also offers significant potential for the high-spatial-resolution mapping of Li distribution in Li-ion battery materials.

Acknowledgement

The NanoSIMS was funded by UK Research Partnership Investment Funding (UKRPIF) Manchester RPIF Round 2. This work was supported by the Henry Royce Institute for Advanced Materials, funded through EPSRC grants EP/R00661X/1, EP/S019367/1, EP/P025021/1 and EP/P025498/1.

References

- (1) Yabuuchi, N.; Yoshii, K.; Myung, S.T.; Nakai, I.; Komaba, S. Detailed Studies of a High-Capacity Electrode Material for Rechargeable Batteries, Li_2MnO_3 – $\text{LiCo}_{1/3}\text{Ni}_{1/3}\text{Mn}_{1/3}\text{O}_2$. *J. Am. Chem. Soc.* **2011**, *133* (12), 4404–4419.
- (2) Lee, J. T.; Nitta, N.; Benson, J.; Magasinski, A.; Fuller, T. F.; Yushin, G. Comparative Study of the Solid Electrolyte Interphase on Graphite in Full Li-Ion Battery Cells Using X-Ray Photoelectron Spectroscopy, Secondary Ion Mass Spectrometry, and Electron Microscopy. *Carbon N. Y.* **2013**, *52*, 388–397.
- (3) Li, J. T.; Swiatowska, J.; Maurice, V.; Seyeux, A.; Huang, L.; Sun, S. G.; Marcus, P. XPS and ToF-SIMS Study of Electrode Processes on Sn–Ni Alloy Anodes for Li-Ion Batteries. *J. Phys. Chem. C* **2011**, *115* (14), 7012–7018.
- (4) Esposto, F. J.; Zhang, C.S.; Norton, P. R.; Timsit, R. S. Segregation Studies of an Al-Li Alloy. *Surf. Sci.* **1993**, *290* (1–2), 93–102.

- (5) Tao, Y.; Ni, D. R.; Xiao, B. L.; Ma, Z. Y.; Wu, W.; Zhang, R. X.; Zeng, Y. S. Origin of Unusual Fracture in Stirred Zone for Friction Stir Welded 2198-T8 Al-Li Alloy Joints. *Mater. Sci. Eng. A* **2017**, *693*, 1–13.
- (6) Degreve, F.; Dubost, B.; Dubus, A.; Thorne, N. A.; Bodart, F.; Demortier, G. Quantitative Analysis of Intermetallic Phases in Al-Li Alloys by Electron, Ion and Nuclear Microprobes. *Le J. Phys. Colloq.* **1987**, *48* (C3), C3-505.
- (7) Soni, K. K.; Williams, D. B.; Newbury, D. E.; Chi, P.; Downing, R. G.; Lamaza, G. Depth Distribution of Lithium in Oxidized Binary Al-Li Alloys Determined by Secondary Ion Mass Spectrometry and Neutron Depth Profiling. *Corrosion* **1993**, *49* (1), 31–41.
- (8) Shim, J. H.; Lee, J.; Han, S. Y.; Lee, S. Synergistic Effects of Coating and Doping for Lithium Ion Battery Cathode Materials: Synthesis and Characterization of Lithium Titanate-Coated LiCoO₂ with Mg Doping. *Electrochim. Acta* **2015**, *186*, 201–208.
- (9) Sui, T.; Song, B.; Dluhos, J.; Lu, L.; Korsunsky, A. M. Nanoscale Chemical Mapping of Li-Ion Battery Cathode Material by FIB-SEM and TOF-SIMS Multi-Modal Microscopy. *Nano Energy* **2015**, *17*, 254–260.
- (10) Burgess, S.; Li, X.; Holland, J. High Spatial Resolution Energy Dispersive X-Ray Spectrometry in the SEM and the Detection of Light Elements Including Lithium. *Microsc. Anal.* **2013**, *6*, S8–S13.
- (11) Wang, Z.; Santhanagopalan, D.; Zhang, W.; Wang, F.; Xin, H. L.; He, K.; Li, J.; Dudney, N.; Meng, Y. S. In Situ STEM-EELS Observation of Nanoscale Interfacial Phenomena in All-Solid-State Batteries. *Nano Lett.* **2016**, *16* (6), 3760–3767.
- (12) Devaraj, A.; Gu, M.; Colby, R.; Yan, P.; Wang, C. M.; Zheng, J. M.; Xiao, J.; Genc, A.; Zhang, J. G.; Belharouak, I. Visualizing Nanoscale 3D Compositional Fluctuation of Lithium in Advanced Lithium-Ion Battery Cathodes. *Nat. Commun.* **2015**, *6* (1), 1–8.

- (13) Li, K.; Liu, J.; Grovenor, C. R. M.; Moore, K. L. NanoSIMS Imaging and Analysis in Materials Science. *Annu. Rev. Anal. Chem.* **2020**, *13*.
- (14) Williams, P. Secondary Ion Mass Spectrometry. *Annu. Rev. Mater. Sci.* **1985**, *15* (1), 517–548.
- (15) Benninghoven, A.; Rudenauer, F. G.; Werner, H. W. Secondary Ion Mass Spectrometry: Basic Concepts, Instrumental Aspects, Applications and Trends. **1987**.
- (16) Jiao, C.; Pillatsch, L.; Mulders, J.; Wall, D. Three-Dimensional Time-of-Flight Secondary Ion Mass Spectrometry and DualBeam FIB/SEM Imaging of Lithium-Ion Battery Cathode. *Microsc. Microanal.* **2019**, *25* (S2), 876–877.
- (17) Dowsett, D.; Wirtz, T. Co-Registered in Situ Secondary Electron and Mass Spectral Imaging on the Helium Ion Microscope Demonstrated Using Lithium Titanate and Magnesium Oxide Nanoparticles. *Anal. Chem.* **2017**, *89* (17), 8957–8965.
- (18) Wirtz, T.; De Castro, O.; Audinot, J. N.; Philipp, P. Imaging and Analytics on the Helium Ion Microscope. *Annu. Rev. Anal. Chem.* **2019**, *12*, 523–543.
- (19) Levi-Setti, R.; Wang, Y. L.; Crow, G. High Spatial Resolution SIMS with the UC-HRL Scanning Ion Microprobe. *Le J. Phys. Colloq.* **1984**, *45* (C9), C9-197.
- (20) Williams, D. B.; Levi-Setti, R.; Chabala, J. M.; Newbury, D. E. High Spatial Resolution Secondary Ion Imaging and Secondary Ion Mass Spectrometry of Aluminium-lithium Alloys. *J. Microsc.* **1987**, *148* (3), 241–252.
- (21) Ma, Y.; Zhou, X.; Thompson, G. E.; Hashimoto, T.; Thomson, P.; Fowles, M. Distribution of Intermetallics in an AA 2099-T8 Aluminium Alloy Extrusion. *Mater. Chem. Phys.* **2011**, *126* (1–2), 46–53.